The Atlantic Multidecadal Oscillation in twentieth century climate simulations: uneven progress from CMIP3 to CMIP5

**Alfredo Ruiz-Barradas · Sumant Nigam ·
Argyro Kavvada**

Abstract Decadal variability in the climate system from the Atlantic Multidecadal Oscillation (AMO) is one of the major sources of variability at this temporal scale that climate models must properly incorporate because of its climate impact. The current analysis of historical simulations of the twentieth century climate from models participating in the CMIP3 and CMIP5 projects assesses how these models portray the observed spatiotemporal features of the sea surface temperature (SST) and precipitation anomalies associated with the AMO. A short sample of the models is analyzed in detail by using all ensembles available of the models CCSM3, GFDL-CM2.1, UKMO-Had-CM3, and ECHAM5/MPI-OM from the CMIP3 project, and the models CCSM4, GFDL-CM3, UKMO-HadGEM2-ES, and MPI-ESM-LR from the CMIP5 project. The structure and evolution of the SST anomalies of the AMO have not progressed consistently from the CMIP3 to the CMIP5 models. While the characteristic period of the AMO (smoothed with a binomial filter applied fifty times) is underestimated by the three of the models, the e-folding time of the autocorrelations shows that all models underestimate the 44-year value from observations by almost 50 %. Variability of the AMO in the 10–20/70–80 year ranges is overestimated/underestimated in the models and the variability in the 10–20 year range increases in three of the models from the CMIP3 to the CMIP5 versions. Spatial variability and correlation of the AMO regressed precipitation and SST anomalies in summer and fall indicate that models are not up to the task of simulating the AMO impact on the hydroclimate over the neighboring continents. This is in spite of the fact that the spatial variability and correlations in the SST anomalies improve from CMIP3 to CMIP5 versions in two of the models. However, a multi-model mean from a sample of 14 models whose first ensemble was analyzed indicated there were no improvements in the structure of the SST anomalies of the AMO or associated regional precipitation anomalies in summer and fall from CMIP3 to CMIP5 projects.

1 Introduction

Decadal climate prediction has taken a prominent role for the first time in the experiments of the Coupled Model Intercomparison Project Phase 5 (CMIP5; Taylor et al. 2011). The need for useful decadal predictions has been made not only from scientific papers (e.g., Meehl et al. 2009; Hurrell et al. 2010), but also from the impact of climate-related events like the current melting of the Greenland glaciers, the ongoing drought in northern Mexico and central US, as well as past decade-long droughts over the same region in the recent twentieth century and over western Africa. Properties of the components of the climate system determine the time scales of the variations within the system: days to weeks for the atmosphere, weeks to years for the biosphere, months to decades for the ice, and months to decades to centuries for the oceans. Thus, perturbations to the slower climate system components can produce climate variability at these long timescales. Therefore, if one aspires to have reliable decadal

A. Ruiz-Barradas (✉) · S. Nigam · A. Kavvada
Department of Atmospheric and Oceanic Science,
University of Maryland, College Park, 3435 Computer and
Space Science Building, College Park, MD 20742-2425, USA
e-mail: alfredo@atmos.umd.edu

predictions, climate models have to properly incorporate the processes that give rise to decadal variability in specific components of the climate system, in addition to the mechanisms through which these processes impact the surface climate affecting human societies.

Phenomena with defined decadal variability that climate models must properly include are the Pacific Decadal Oscillation (PDO, Mantua et al. 1997) and the Atlantic Multidecadal Oscillation (AMO, Enfield et al. 2001; Guan and Nigam 2009). However, it is not always clear what drives a given phenomenon, as it is the case of the AMO. One of the most accepted theories relates the Atlantic sea surface temperature (SST) fluctuations to variations in the Atlantic Meridional Overturning Circulation (Latif et al. 2004; Medhaug and Furevik 2011; Zhang et al. 2013), but one of the newest and most controversial relates the SST variations to fluctuations in atmospheric concentrations of anthropogenic and natural aerosols (Evan et al. 2009; Booth et al. 2012). Decadal control of hydroclimate from the AMO over North America and Africa is one of the main reasons to worry about having this phenomenon properly incorporated in climate models. Multi-year, summer and fall droughts over North America and Africa have been observationally linked to decadal SST variability in the Atlantic (e.g., Enfield et al. 2001; Ruiz-Barradas and Nigam 2005; Wang et al. 2006; Zhang and Delworth 2006; McCabe et al. 2008; Shanahan et al. 2009; Kushnir 2010; Nigam et al. 2011).

The focus of the paper is not to unveil the nature of the AMO or assess its predictability but to provide a comparison of the capabilities of the current state-of-the-art models in simulating the AMO. In other words, the main goal of this paper is to assess the way models from the CMIP3 and CMIP5 projects depict the AMO in the twentieth century climate, an important component of decadal variability on the climate system, and a key element for decadal prediction. This evaluation will provide elements to find out if AMO-like decadal variability, of great importance for hydroclimate variability over North America and Africa, has improved in the latest CMIP5 models over those from the CMIP3 project. A detailed analysis of the spatiotemporal features of the AMO in the atmosphere and ocean, and its hydroclimate impact over North America, in CMIP5 models has already been carried out (Kavvada et al. 2013), so the focus here will be on the model inter-comparison and assessment against observations.

The paper is divided as follows. Section 2 gives information on the models, simulations and observations used as well as the methods employed in the assessment. Section 3 assesses the spatiotemporal features of the AMO-related SST anomalies. Section 4 evaluates temporal variability and correlation of the AMO indices, and spatial variability and correlation of AMO-related precipitation and SST anomalies in summer and fall. Finally Sect. 5 gives some concluding remarks.

2 Data sets

The present analysis uses SSTs and precipitation from observations and simulations of the twentieth century climate from models participating in CMIP3 and CMIP5 projects for the Intergovernmental Panel on Climate Change (IPCC). Observed SST data comes from the UK. Met office's Hadley Centre Sea Ice and Sea Surface Temperature dataset, version 1.1 (HadISST 1.1, Rayner et al. 2003). On the other hand observed precipitation is obtained from the University of East Anglia Climate Research Unit high resolution gridded data analysis of station data, version 3.1 (CRUTS3.1; Mitchell and Jones 2005). While the main analysis is carried on with a selected set of models, a complementary analysis is done with an extended set of models. The models used in the main analysis come from leading international climate research centers from the US, NCAR and NOAA's GFDL, the UK. Met Office Hadley Centre, and the German Max Plank Institute for Meteorology (MPI-M). On the other hand, the larger set of models used in the complementary analysis are models that participated in the CMIP3 project and were also used in an updated version in the CMIP5 project. The historical simulations analyzed are run by imposing changing conditions, consistent with observations, which may have included: atmospheric composition, due to both anthropogenic and volcanic influences, solar forcing, emissions or concentrations of short-lived species and natural and anthropogenic aerosols as well as land use.

2.1 CMIP3 models

The CMIP3 models analyzed include: (1) version 3 of NCAR's Community Climate System Model CCSM3 (Collins et al. 2006, and additional references in the CCSM special issue in the Journal of Climate), (2) version 2.1 of NOAA's GFDL Coupled Climate Model GFDL-CM2.1 (Delworth et al. 2006), (3) version 3 of UK. Meteorological Office and Hadley Centre Coupled Climate Model UKMO-HadCM3 (Gordon et al. 2000; Pope et al. 2000), and (4) Germany's version 5 of European Centre Hamburg Model/MPI-M's Ocean Model ECHAM5/MPI-OM (Roeckner et al. Roeckner et al. 2003; Marsland et al. 2003). The twentieth century climate simulations started from the late nineteenth century and went through 1999 or 2000 with no apparent standardization of the time series of atmospheric composition greenhouse gases and atmospheric aerosols. The CMIP3 models used in the complementary analysis are listed in Table 1.

Table 1 Models used in the complementary analysis from CMIP3 and CMIP5 projects (Fig. 6)

CMIP3 model	CMIP5 model	Model # used in (Fig. 6 d, e)	Institution
–	BCC-CSM1.1	1	Beijing Climate Center, China Meteorological Administration, China
CGCM3.1	CanESM2	2	Canadian Center for Climate Modeling and Analysis, Canada
CCSM3	CCSM4	3	National Center for Atmospheric Research, USA
CNRM-CM53	CNRM-CM5.1	4	National Centre for Meteorological Research, France
CSIRO-MK3.5	CSIRO-MK3.6	5	Commonwealth Scientific and Industrial Research Organization/Queensland Climate Change Centre of Excellence, AUS
GFDL-CM2.1	GFDL-CM3	6	NOAA Geophysical Fluid Dynamics Laboratory, USA
–	GFDL-ESM2G/M	7	NOAA Geophysical Fluid Dynamics Laboratory, USA
GISS-ER	GISS-E2-H/R	8	NASA Goddard Institute for Space Studies, USA
UKMO-HadCM3	UKMO-HadCM3	9	Met Office Hadley Centre, UK
CMIP3 model	CMIP5 model	Model # used in (Fig. 6d, e)	Institution
UKMO-HadGEM1	UKMO-HadGEM2-ES	10	Met Office Hadley Centre, UK
INMCM3	INMCM4	11	Institute for Numerical Mathematics, Russia
IPSL-CM4	IPSL-CM5A-LR	12	Institute Pierre Simon Laplace, France
MIROC3.2	MIROC5	13	Japan Agency for Marine-Earth Science and Technology, Atmosphere and Ocean Research Institute (The University of Tokyo), and National Institute for Environmental Studies
–	MIROC-ESM	14	Japan Agency for Marine-Earth Science and Technology, Atmosphere and Ocean Research Institute (The University of Tokyo), and National Institute for Environmental Studies
ECHAM5/MPI-OM	MPI-ESM-LR	15	Max Planck Institute for Meteorology, Germany
MRI-CGCM2	MRI-CGCM3	16	Meteorological Research Institute, Japan
BCCR-BCM2	NorESM1-M	17	CMIP3: Bjerknes Centre for Climate Research, Norway CMIP5: Norwegian Climate Center, Norway

2.2 CMIP5 models

The CMIP5 models analyzed include: (1) version 4 of NCAR's Community Climate System Model CCSM4 (Gent et al. 2011), (2) version 3 of NOAA's GFDL Coupled Climate Model GFDL-CM3 (Donner et al. 2011; Griffies 2011), (3) UKMO Hadley Centre Global Environment Model version 2, I nits earth system configuration, UKM-HadGEM2-ES (Collins et al. 2008), and (4) Germany's version 6 of European Centre Hamburg Model/MPI-M's Earth System Model, low resolution version, ECHAM6/MPI-ESM-LR (Raddatz et al. 2007; Marsland et al. 2003). The historical twentieth century climate simulations started from the mid nineteenth century and finished in 2005, but unlike the CMIP3 simulations, the forcing was standardized for all models. Note that the CMIP5 versions of the models from NCAR and GFDL are updated versions of the CMIP3 models, but the CMIP5 versions of the models from UKMO and MPI are Earth System models. The CMIP5 models used in the complementary analysis are listed in Table 1.

2.3 Methods

The current analysis is based on seasonal data. Seasons are defined in terms of their boreal hemisphere 3-month means: winter, December–February; spring, March–May; summer, June–August; and fall, September–November. Seasonal anomalies were created by extracting the long-term mean (1900–1999). AMO indices were generated by taking the spatial average of SST anomalies in the Atlantic domain (5–75°W and 0–60°N), and then linearly detrended by using the least squares method; the index is then smoothed by applying a (1-2-1) binomial filter 50 times which preserves the decadal-to-interdecadal variability. Smoothed versions of the AMO index are generated for

observations and each ensemble member available for the models. Lead/lag regression and correlation analyses are then used to investigate the spatial and temporal structures associated with the smoothed AMO in observations and model simulations of the twentieth century climate. Model results are presented as the mean of the all-season regressions/correlations of the different ensemble members in each model, and are compared against all-season regressions/correlations from observations in Sect. 3 and the first part of Sect. 4, while summer and fall regressions/correlations are used in the second part of Sect. 4. The number of ensembles used in each of the CMIP3 and CMIP5 models is: 8 for CCSM3 and 6 for CCSM4, 3 for GFDL-CM2.1 and 5 for GFDL-CM3, 2 and 4 for UKMO-HadGEM2-ES, and 4 for ECHAM5/MPI-OM and 3 for ECHAM5/MPI-ESM-LR. The complementary analysis with the extended set of models relies on the first ensemble member only of the historical simulations.

3 Features of the Atlantic Multidecadal Oscillation

3.1 Structure

The warm phase of the mature AMO is characterized by maximum SST anomalies in the north Atlantic, to the south of Greenland and to the east of Newfoundland, and a secondary maximum on the northern tropical Atlantic in front of the Western African coasts; the secondary maximum is enclosed for a subtropical/tropical extension of the anomalies over the north Atlantic (Fig. 1a) that reaches the Caribbean Sea and leaves under normal conditions the Gulf of Mexico and western Sargasso Sea. The focus of the SST anomalies on the region of the sub-polar gyre, where major water masses pass from/to higher latitudes, suggests these anomalies may be more than the response to atmospheric conditions and be linked to subsurface ocean processes involving heat content and salinity anomalies as well (Kavvada et al. 2013). Thus, a reasonable depiction of the observed structure of the AMO by the models may suggest that the underlying processes that generate the AMO are reasonably incorporated.

Analysis of the structure of the AMO-related SST anomalies in the twentieth century climate simulations from the CMIP3 models (Fig. 1b, d, f, h) emphasizes that the region with the largest anomalies are in the Labrador Sea. This region, that is to the northwest of the region of maximum anomalies in observations, has maximum SST anomalies in all models, however, the maximum has an eastward extension in CCSM3 that is placed to the south of Iceland over the northern half of the sub-polar North Atlantic; in any case, the models are misplacing the maximum SST anomalies found in observations. Only CCSM3

depicts negative anomalies in front of Newfoundland over the region of the Grand Banks which are not present in observations. It is also noted that models tend to put SST anomalies to the north of Iceland, which are not present in observations.[1] The secondary maximum of SST anomalies in the northern tropical Atlantic found in observations is absent from the model simulations, however, the models produce the subtropical/tropical extension of the northern anomalies with a varied degree of success. While the southward extension in CCSM3 and GFDL-CM2.1 models barely reaches the 20°N line, it reaches the deep tropics and Caribbean Sea as in observations in UKMO-HadCM3 and ECHAM5/MPI-OM models. It is interesting to note that while the tropical Pacific has climatological conditions (or close to zero anomalies) associated to the AMO in observations, SST anomalies over that region from the model simulations are extensive.

The Labrador Sea focus in the structure of the AMO-related SST anomalies seen in CMIP3 models is reduced in CMIP5 models (Fig. 1c, e, g, i); this is more evident in CCSM4. Models also tend to place the maximum SST anomalies farther to the east than observed; these anomalies are in the range of the observed anomalies. Except for the GFDL-CM3 model, all the other models show negative anomalies in front of Newfoundland over the region of the Grand Banks which are no existent in observations. The anomalies to the north of Iceland have also been reduced in the CMIP5 models, except by the CCSM4 model which present the largest anomalies over the Greenland Sea. The structure of the northern tropical Atlantic anomalies still have marked deficiencies; while CCSM4 has no tropical component at all, and ECHM6/MPI-ESM-LR has reduced its extension, GFDL-CM3 has extended it into the deep tropical Atlantic, and UKMO-HadGEM2-ES has increased its magnitude as in observations. The fictitious tropical Pacific signature of the AMO in the models has increased in GFDL-CM3 and CCSM4, but it is reduced in the other two models. From these models, UKMO-HadGEM2-ES seems to be in better accord with observations, while CCSM4 is the one with the most obvious deficiencies.

3.2 Characteristic period

The period of the AMO indices can be obtained via their autocorrelation functions (Fig. 2). The crossing of the observation-based AMO autocorrelation (thick black line) with the zero line shows a dominant period of approximately 56 years (the intersection point allows for an estimate of the time series' half-period). The continuous

---

[1] The region is data-sparse but not data-void, and the quality of the data when compared with in situ data is reasonable according to an analysis made by Hughes et al. (2009).
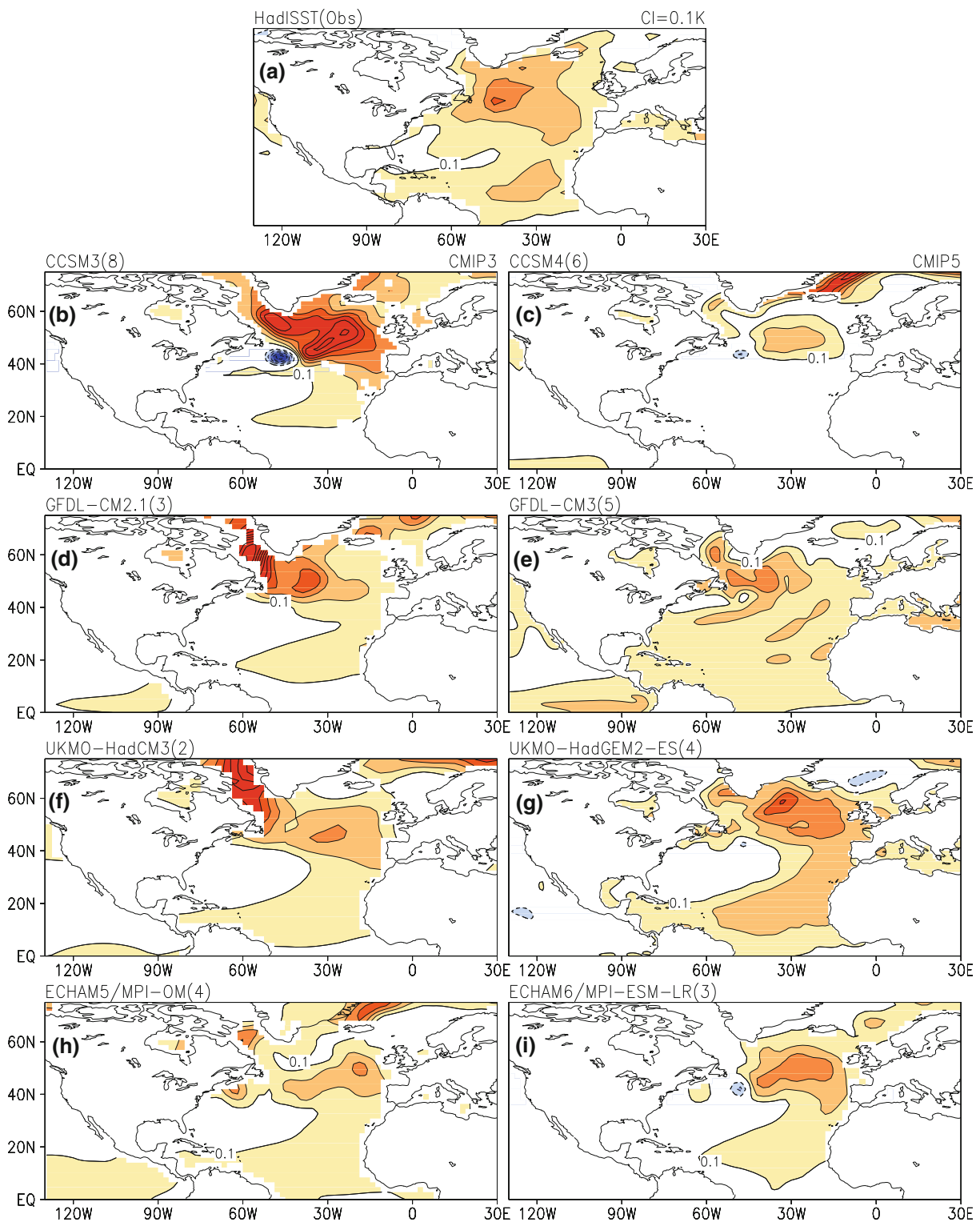
Fig. 1 All-season regressions of smoothed AMO indices on corresponding SST anomalies in observations (*top*), CMIP3 (*left panels*) and CMIP5 (*right panels*) climate simulations for the period 1900–1999. **a** Observed regressed anomalies from HadISST; mean regressed anomalies from CMIP3 simulations from **b** CCSM3, **d** GFDL-CM2.1, **f** UKMO-HadCM3, and **h** ECHAM5/MPI-OM models; mean regressed anomalies from CMIP5 simulations from **c** CCSM4, **e** GFDL-CM3, **g** UKMO-HadGEM2-ES, and **i** ECHAM6/MPI-ESM-LR models. Regressions from model simulations were calculated for all the ensembles available for a given model, then the mean regression was calculated; the *number in parenthesis* denotes the number of ensembles used from each model to generate the mean regressed anomalies. *Yellow-to-red/blue shading* denotes positive/negative SST anomalies plotted with a 0.1 K contour interval

colored lines representing the mean autocorrelation for each of the CMIP5 models (Fig. 2a) display a general underestimation of the AMO period: 40 years in ECHAM6/MPI-ESM-LR, 44 years in GFDL-CM3, and 52 years in CCSM4; however the period is 68 years in UKMO-HadGEM2-ES. It is interesting to point out that if the temporal comparison is done using the time needed for the autocorrelation to decay to 1/e of its value models are farther apart from observations: while observations indicate a 44 year de-correlation period, models are grouped together around the 16–24 years range! Note that these estimations of the time scale of the smoothed AMO tend to be shorter than others using heavier filters that maximize the low frequency modulation of the decadal pulses (e.g. Enfield et al. 2001; Ting et al. 2011).

Comparison of the AMO autocorrelations from CMIP5 models with the corresponding from the CMIP3 models does not show a marked difference between the associated periods of the AMO (Fig. 2b–e), except in the case of the UKMO models whose period went from a 16 year period in the CMIP3 model to a 68 year period in the CMIP5 model. De-correlation times decreased in the CMIP5 versions of the NCAR, GFDL and MPI models, while it increased in the UKMO models.

The integrated view of the autocorrelation of the smoothed AMO indices can be expanded via the spectral analysis of the time series (Fig. 3) to provide a deeper insight into what may be behind the variability in observations and models. It is clear that both sets of CMIP3 and CMIP5 models underestimate low frequency variability in the 70–80 and 30–40 year ranges while overestimate variability in the 10-20 year range. Variability in the 10–20 year range has increased, and exceeded that variability from observations, in GFDL, UKMO and MPI CMIP5 models with respect to the CMIP3 models, but not in the NCAR models. Conversely, variability in the 70–80 years range has increased, but it is still under that variability from observations in GFDL, UKMO and MPI CMIP5 models with respect to the CMIP3 models, but decreased significantly in the NCAR models.

3.3 Evolution

A more complete view of the surface features of the AMO is reached by displaying the evolution of the SST anomalies around the mature stage via all-season lead/lag regressions (Fig. 4). During the warm phase of the AMO positive SST anomalies emerge from the Davis Strait and Labrador Sea in observations (Fig. 4a) and follow a southeastward propagation in the higher mid-latitudes and a subsequent southwestward displacement toward the lower latitudes which track the east branch of the subtropical gyre as time progresses until they reach maximum

Fig. 2 Autocorrelations of the smoothed AMO indices from observations and CMIP3 (*dashed lines*) and CIMP5 (*continuous lines*) climate simulations for the period 1900–1999. Autocorrelations from observations come from HadISST (*black*), mean autocorrelations from CMIP5 simulations come from CCSM4 (*continuous red*), GFDL-CM3 (*continuous green*), UKMO-HadCM3 (*continuous blue*), and ECHAM6/MPI-ESM-LR (*continuous violet*) models, while mean autocorrelations from CMIP3 simulations come from CCSM3 (*dashed red*), GFDL-CM2.1 (*dashed green*), UKMO-HadCM3 (*dashed blue*), and ECHAM5/MPI-OM (*dashed violet*) models. **a** Autocorrelations from observations and CMIP5 simulations, mean autocorrelations from **b** CCSM4 and CCSM3 simulations, **c** GFDL-CM3 and GFDL-CM2.1 simulations, **d** UKMO-HadCM3 and UKMO-HadGEM2-ES simulations, and **e** ECHAM5/MPI-OM and ECHAM6/MPI-ESM-LR simulations. Autocorrelations from AMO indices from model simulations were calculated for all the ensembles available for a given model, then the mean autocorrelation and the standard deviation among the ensembles were calculated; the *number in parenthesis* denotes the number of ensembles used from each model to generate the mean autocorrelation, while the *error bars* represent the standard deviation. The *thin gray line* represents the 1/e value used to visually estimate the e-folding time of the correlations. The *x*-axis is given in years

amplitude and extension in the mature state; the subtropical anomalies are weaker than those in the mid-latitudes, with a local maximum developing off the western Africa coasts. Anomalies gradually decrease in magnitude, with the signal first dissipating over the tropical latitudes and subsequently further to the north.

The structure and evolution around the mature stage of the SST anomalies associated with the warm phase of the AMO in the models have only a general agreement with observations and have marked differences between the CMIP3 and CMIP5 versions. All modeled SST anomalies associated with the AMO reach maximum values and extension at the mature phase, as in observations, without consideration of the type of model. However the magnitude of the anomalies and structure in general do not match those from observations. The CMIP5 version of the NCAR model, CCSM4, changed dramatically the magnitude and structure of the SST anomalies displayed by the CMIP3 version of the model, CCSM3 (Fig. 4b, c): while CCSM3 has a similar propagation to the one in observations originating over the Labrador Sea and anomalies reach a maximum extension on the northern tropical Atlantic, the anomalies from CCSM4 seem to originate over the Greenland Sea and never reach tropical latitudes. The CMIP5 version of the GFDL model, GFDL-CM3, also exhibits notable changes of the AMO-related SST anomalies when compared with the corresponding from its CMIP3 version, GFDL-CM2.1 (Fig. 4d, e): while GFDL-CM2.1 has little propagation of the anomalies over the Labrador Sea and anomalies reach tropical latitudes in the mature stage, the anomalies from GFDL-CM3 are smaller, propagate more actively in the mid-latitudes, and reach tropical latitudes 2 years before and after the mature stage
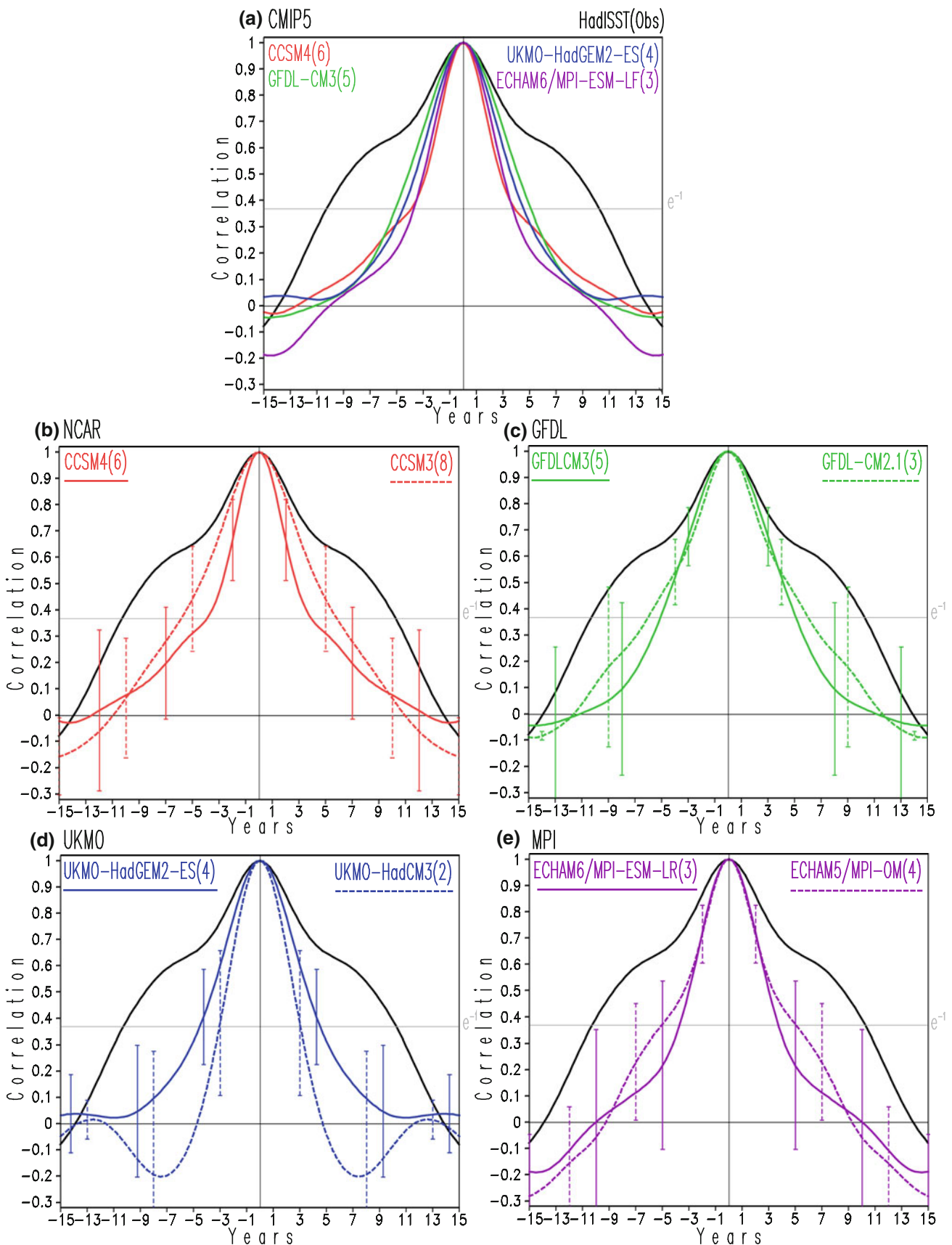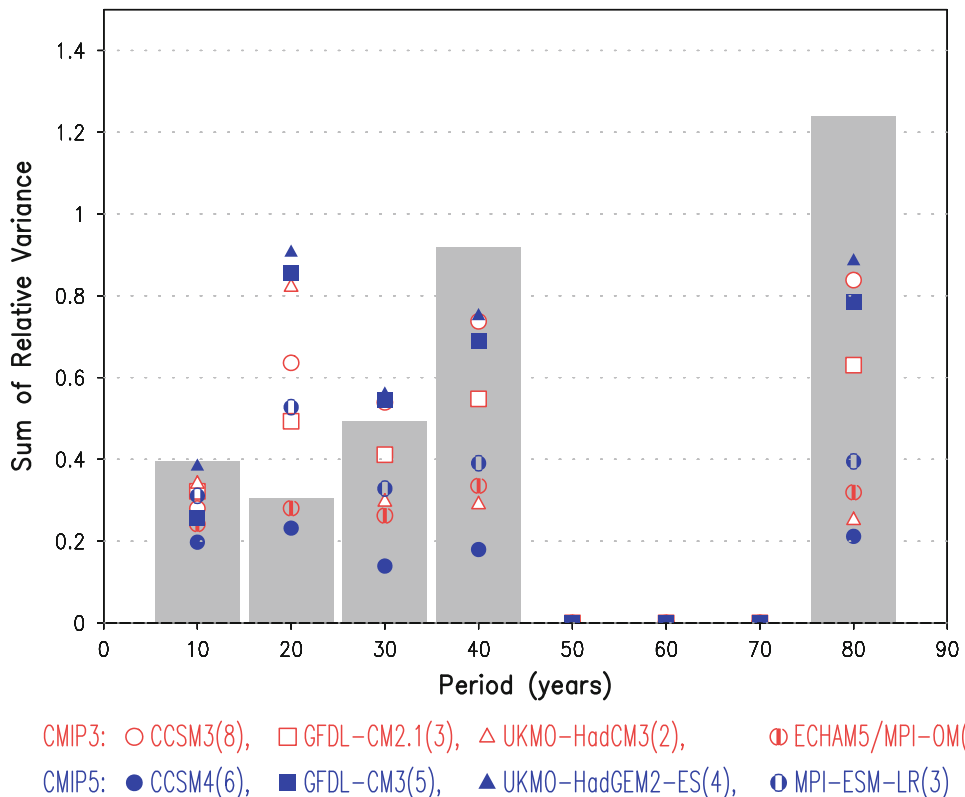
Fig. 3 Histogram of mean spectral analysis peaks from spectral analyses of smoothed AMO indices for the period 1900–1999. The *y*-axis denotes the sum of relative variance in the following ranges 2.5–10 years, 11–20 years, 21–30 years, 31–40 years, and 71–80 years. Spectral peaks from the AMO index from observations are shown with the *gray bars*; the corresponding peaks for the CMIP5 models are shown by the *symbols* in *blue*, and those for the CMIP3 models are in *red*; see legend to identify particular models. The *number* in *parenthesis* denotes the number of ensembles used for each model. Spectral analyses were calculated for each ensemble member, and then a mean spectrum was obtained by averaging the spectrum of the ensembles for each model

similarly to observations, but their structures have some differences, including anomalies over the eastern tropical Pacific and negative anomalies over the Labrador Sea 2 and 4 years after the mature state which are not seen in observations. The CMIP5 version of the UKMO model, UKMO-HadGEM2-ES, similarly to the GFDL model, also has some changes on the SST anomalies when compared with those from its CMIP3 version, UKMO-HadCM3 (Fig. 4f, g): while UKMO-HadCM3 has anomalies with little change over the Labrador Sea, with anomalies that reach the tropical latitudes in the mature state and linger just off the African coasts 2 years after it, the anomalies from the UKMO-HadGEM2-ES are smaller, and propagate in the mid-latitudes and reach the tropical latitudes 2 years before and after the mature stage as in observations; UKMO-HadGEM2-ES is the only model that reproduces the magnitude of the observed AMO-related anomalies in the tropical North Atlantic as well as their structure in the mature stage and 2 years before and after it, although negative anomalies are evident over the Greenland Sea which are not displayed in observations. The CMIP5 version of the MPI model, MPI-ESM-LR, is not the exception

and also has changes when the AMO-related anomalies are compared with those from the CMIP3 version, ECHAM5/MPI-OM (Fig. 4h, i): while ECHAM5/MPI-OM has the largest anomalies over the Greenland Sea and anomalies reach the tropical latitudes only in the mature stage, the MPI-ESM-LR reduces the anomalies over the Greenland Sea, increases the anomalies in the mid-latitudes but reduces the extension of the tropical anomalies in the mature state.

4 Assessment

An objective way to compare the temporal and spatial features of the smoothed AMO indices and regressed precipitation and SST anomalies can be achieved by the use of Taylor diagrams (Fig. 5). Comparison of the temporal features of the AMO indices (Fig. 5a) indicates the majority of the models have poor correlation with observations and under-estimate the observed variability, except for the GFDL and the UKMO-HadGEM2-ES models. While the CMIP5 version of the GFDL model improves the
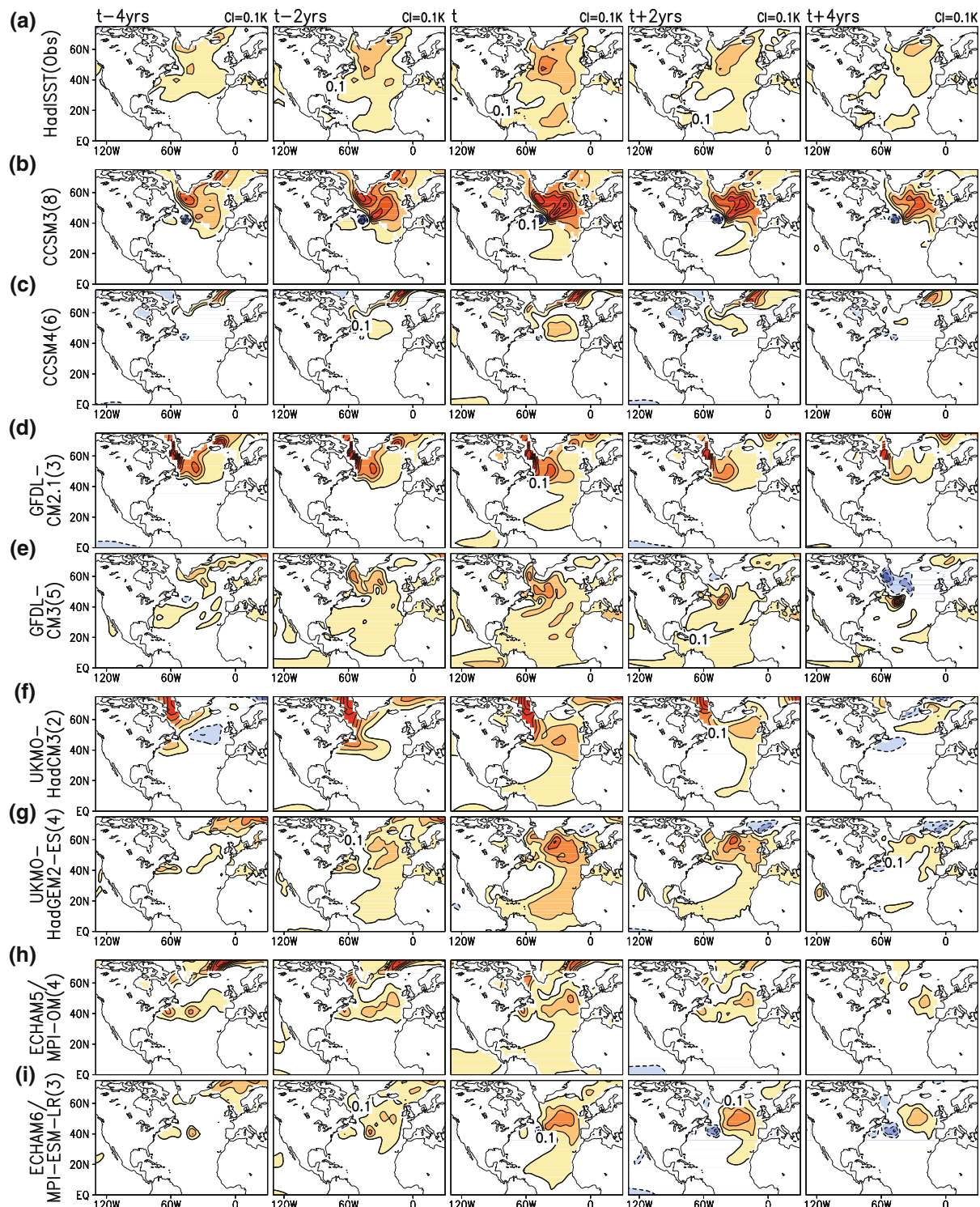
Fig. 4 Lead/lag regressions of the all-season smoothed AMO indices on SST anomalies from observations and CMIP3 and CMIP5 climate model simulations for the period 1900–1999. The *first two columns* display regressions 4 and 2 years in advance of the mature phase of the AMO (t-4 years and t-2 years respectively), the *center column* displays the mature phase (t), and the *last two columns* display regressions 2 and 4 years after the mature phase of the AMO (t_2 years and t + 4 years). Regressed anomalies from **a** HadISST observations, **b** CMIP3's CCSM3, **c** CMIP5's CCSM4, **d** CMIP3's GFDL-CM2.1, **e** CMIP5's GFDL-CM3, **f** CMIP3's UKMO-HadCM3, **g** CMIP5's UKMO-HadGEM2-ES, **h** CMIP3's ECHAM5/MPI-OM, and **i** CMIP5's MPI-ESM-LR simulations. Regressions from model simulations were calculated for all the ensembles available for a given model, then the mean regression was calculated; the *number in parenthesis* denotes the number of ensembles used from each model to generate the mean regressed anomalies. *Yellow*-to-*red*/*blue* shading denotes positive/negative SST anomalies plotted with a 0.1 K contour interval

variability of the smoothed AMO index from the CMIP3 version, it slightly decreases the correlation with the observed index; on the other hand, the CMIP5 version of the UKMO model greatly improves the variability as well as the correlation with the observed index.

Comparison of the spatial variability from the regressed precipitation and SST anomalies on the smoothed AMO indices is carried on summer and fall, the seasons when the AMO impacts the most the regional hydroclimate. It is clear that the models are not up to the task of simulating the impact of the regional hydroclimate yet (Fig. 5b, c): the spatial variability of the precipitation anomalies is under-estimated, and the spatial correlations with observations are under 0.3 over the North American domain in either season. On the other hand, the spatial variability and spatial correlations in the SST anomalies improve from CMIP3 to CMIP5 versions of the MPI and UKMO models, being the most successful the UKMO-HadGEM2-ES model in both seasons; the most dramatic degeneration, is in the NCAR models.

While the previous analysis uses the ensembles available of four models, the ensuing comparison uses the first ensemble of a larger sample of CMIP3 and CMIP5 models. Smoothed indices for the AMO were created for each of the models and regressed on SST and precipitation in summer and fall. Regressions from observations, multi-model means and their differences with observations are shown in Fig. 6a–c. Observations indicate that SST anomalies increase in the midlatitudes from summer to fall but decrease in extension in the northern tropical Atlantic. Concomitant to the seasonal evolution of oceanic anomalies is the deficit in precipitation over North America in summer, which expands and intensifies from northern Mexico to the US in fall; on the other hand, western Africa experiences wet conditions in both seasons. Both CMIP3 and CMIP5 multi-model means do not simulate the intensification of SST anomalies over the Mid Atlantic from summer to fall, and are colder than observations indicate, especially in fall. The associated impact on the regional precipitation anomalies in the multi-model means show increased precipitation in summer and a very weak deficit in precipitation in fall over North America. In short, the multi-model means show wetter North America and drier western Africa than observations in summer and fall.

Spatial correlations of the observed and simulated anomalies do not indicate an improvement of the CMIP5 versus CMIP3 models (Fig. 6d, e). While there are some CMIP5 models that perform better than their CMIP3 comparison models (refer to Table 1 to identify the models), their multi-model means have smaller spatial correlations with observations than those from the CMIP3 multi-model means: 0.43/0.58 for SST anomalies (over the oceanic domain displayed in the Fig. 6) from CMIP5/CMIP3 multi-model mean in summer, and 0.38/0.58 in fall; 0.13/ 0.14 and 0.06/0.25 for precipitation anomalies (over the continental domain to the west of 60°W shown in Fig. 6) from CMIP5/CMIP3 in summer and fall respectively.

It is worth to point out that in the context of North America hydroclimate, particularly over the central US, models are unable to properly simulate the impact of the AMO in summer and fall. This is in spite of having the broad oceanic features of the AMO, better in CMIP3 than in CMIP5 multi-model means. Independently of the version, this problem seems to be related to the inability of the models to modify the regional low level circulation that modulates the moisture fluxes affecting the region (Kavvada et al. 2013; Sheffield et al. 2013).

5 Concluding remarks

Decadal variability in the climate system from the AMO is one of the major sources of variability at this temporal scale that climate models must aim to properly incorporate because its surface climate impact on the neighboring continents. This issue has particular relevance for the current effort on decadal climate prediction experiments been analyzed for the IPCC in preparation for the fifth assessment report. The current analysis does not pretend to investigate into the mechanisms behind the generation of the AMO in model simulations, but to provide evidence of improvements, or lack of them, in the portrayal of spatio-temporal features of the AMO from the previous to the currents models participating in the IPCC. If climate models do not incorporate the mechanisms associated to the generation of the AMO (or any other source of decadal variability like the PDO) and in turn incorporate or enhance variability at other frequencies, then the models ability to simulate and predict at decadal time scales will be compromised and so the way they transmit this variability to the surface climate affecting human societies.

The current analysis of historical simulations of the twentieth century climate from state-of-the-art climate models from the CMIP5 and CMIP3 projects assesses how these models portray the structure of the evolving SST anomalies associated with the AMO and its variability. In addition, spatial variability of SST and precipitation anomalies associated with the AMO is evaluated for summer and fall. Comparisons with observations help to establish if the CMIP5 models are improving over their previous CMIP3 versions.

The mature stage of the warm phase of the AMO has evolved from the CMIP3 to the CMIP5 version but it has not progressed consistently through the models. Observations show that the AMO has a maximum of SST anomalies to the south of Greenland and a secondary maximum in the northern tropical Atlantic. The renditions of the
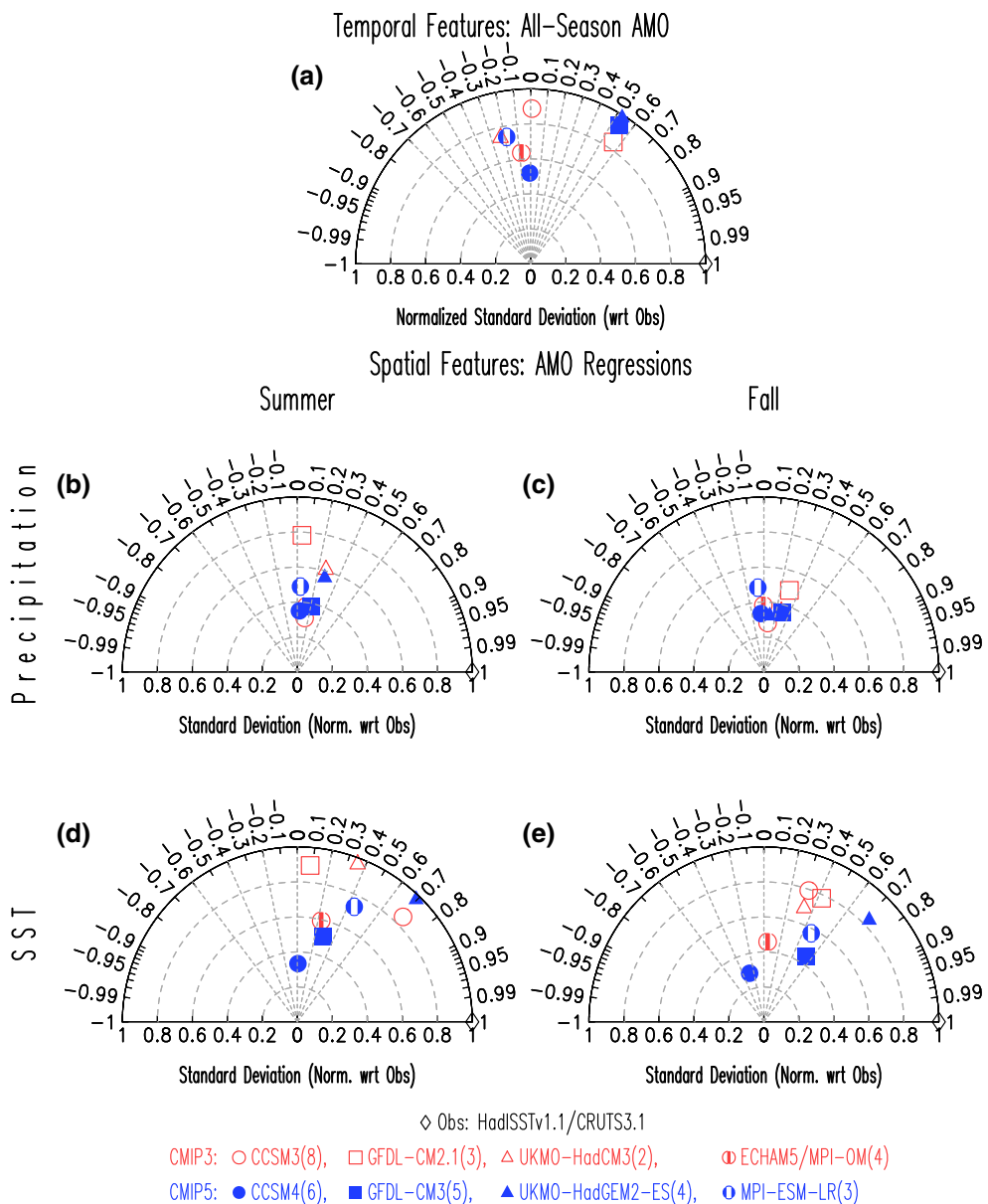
Fig. 5 Taylor diagrams of smoothed AMO indices and their regressions from observations and CMIP3 and CMIP5 climate model simulations for the period 1901–1999. **a** Diagram for temporal features of the all-season smoothed AMO indices; standard deviations have been normalized with respect to the observed standard deviation of 0.17 K. **b** and **c** diagrams for spatial features of regressed continental precipitation anomalies over the (130–60°W, 0–60°N) domain in summer and fall respectively; spatial standard deviations have been normalized with respect to the observed standard deviations in summer, 0.16 mm day^{-1}, and fall, 0.18 mm day^{-1}. **d** and **e** diagrams for spatial features of regressed SST anomalies over the (130°W–10°E, 0–75°N) domain in summer and fall respectively; spatial standard deviations have been normalized with respect to the observed standard deviations in summer, 0.09 K, and fall, 0.10 K. Displayed standard deviations and correlations from models are the means of the different ensembles from each model; the *number* in *parenthesis* denotes the number of ensembles used from each model to generate the mean standard deviation and mean correlation. CMIP3 models are shown in *red symbols*, and CMIP5 models in *blue*

AMO from CMIP3 models have maximum SST anomalies over the Labrador Sea with a secondary maximum to the east of Greenland and weak anomalies over the tropics. The CMIP5 versions of the models in general reduce the double maximum of SST anomalies over the mid-latitudes of the Atlantic to a one maximum southeastward of Greenland and varied representations of the maximum in the tropics: while CCSM4 has no extension over the tropical Atlantic, and GFDL-CM3 highlights more the eastern tropical Pacific than the tropical Atlantic, UKMO-HadGEM2-ES portrays the best the AMO structure, followed by the MPI-ESM-LR.
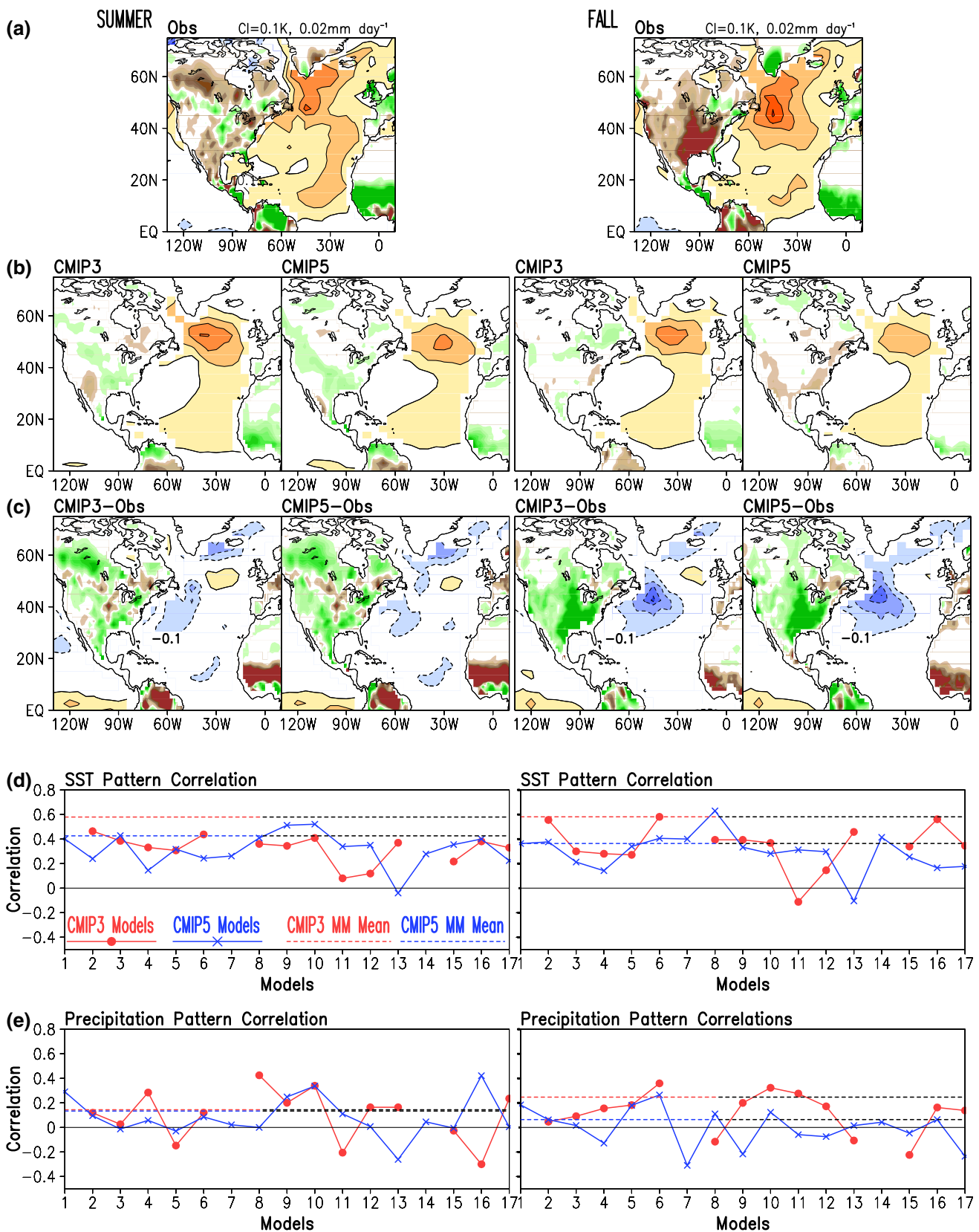
◄ **Fig. 6** Observed and multi-model mean SST and precipitation regressions on smoothed AMO indices and spatial pattern correlations in summer and fall for the period 1901–1999. **a** regressions from observations in summer (*left*) and fall (*right*), **b** mean multi-model regressions from CMIP3 and CMIP5 models in summer (*left panels*) and fall (*right panels*), **c** difference between multi-model mean regressions and observations in summer (*left panels*), and fall (*right panels*). **d** Diagrams for spatial correlations between regressed SST anomalies over the domain (130°W–10°E, 0–75°N) from CMIP3 and CMIP5 models with the corresponding from observations in summer (*left*) and fall (*right*). **e** Diagrams for spatial correlations between regressed continental precipitation anomalies over the domain (130–60°W, 0–60°N) from CMIP3 and CMIP5 models with the corresponding from observations in summer (*left*) and fall (*right*). *Yellow*-to-*red*/*blue shading* denotes positive/negative SST anomalies plotted with a 0.1 K contour interval, and *brown*/*green shading* denotes positive/negative precipitation anomalies with a 0.02 mm day^{-1} interval in panels **a**–**c**. *Lines* in *red*/*blue* denote CMIP3/CMIP5 model correlations in panels **d** and **e**; *continuous lines* with marks are for the individual models while the *dashed lines* are correlations for the multi-model means. Spatial correlations for the regressed SST anomalies from the CMIP5/CMIP3 multi-model means are 0.43/0.58 in summer and 0.36/0.58 in fall, and spatial correlations for the regressed precipitation anomalies from the CMIP5/CMIP3 multi-model means are 0.13/0.14 in summer and 0.06/0.25 in fall

The evolution of the SST anomalies associated with the warm phase of the AMO in models reaches maximum values and extension at the mature stage as in observations but have marked differences in magnitude and structure between the CMIP3 and CMIP5 versions. Anomalies seem to originate along the Davis Strait and Labrador Sea before the mature stage in observations, then propagate southeastward and reach maximum magnitude south of Greenland and extend into the tropics in the mature stage; in the post-mature stages the anomalies over the tropics start to abate and the anomalies in the mid-latitudes move to the east of Greenland. While the CMIP3 models seem to have this general displacement of anomalies originating along the Davis Strait and Labrador Sea, their CMIP5 versions seem to originate over the Greenland Sea. As in the case of the analysis of the mature stage, the evolution of anomalies is captured poorly by CCSM4, and in a better way by UKMO-HadGEM2-ES.

The evolution of the SST anomalies associated with the AMO is closely related to the characteristic period of the AMO in the models. While observations indicate a period close to 56 years, the NCAR, GFDL and MPI CMIP3 and CMIP5 models underestimate this value with periods in the 40–52 years range; the UKMO models however go from an extremely low period close to 16 years in the CMIP3 version, to an overestimation close to 68 years. On the other hand, if the period is judged using the time at which correlations decay to a 1/e of its value, all models underestimate the 44-year value suggested from observations with periods in the 16–24 years range. It is clear that both sets of CMIP3 and CMIP5 models underestimate low

frequency variability in the 70–80 and 30–40 year ranges while overestimate variability in the 10–20 year range. Variability in the higher 10–20 year range increases from CMIP3 to CMIP5 in three of the models surpassing the variability in this range from observations.

The temporal variability and correlations of the AMO indices from the majority of the models are low when compared with the observed AMO index. The exceptions are for the indices from the CMIP5 versions of the GFDL and the UKMO models with variability close to observations and correlations slightly above 0.5. The success of the CMIP5 version of the GFDL model in these assessments of the AMO indices is surprising considering that the structure and the evolution of the SST anomalies were not the best among the models, as it was the case for the CMIP5 version of the UKMO model.

On the other hand, comparison of the observed spatial variability and spatial correlations of the regressed precipitation and SST anomalies of the AMO indices in summer and fall indicates that models are not up to the task of simulating the impact on the regional hydroclimate. The spatial variability and correlations in the SST anomalies improve from CMIP3 to CMIP5 versions of the MPI and UKMO models, being the most successful the UKMO-HadGEM2-ES model in both seasons; the most dramatic degradation is in the NCAR models.

Analysis of AMO regressions from the extended set of models reveals no improvements in the oceanic and hydroclimate impact associated with the AMO from CMIP3 to CMIP5 projects. Pattern correlations with observed SST and precipitation anomalies are smaller in CMIP5 than in CMIP3 models in summer and fall.

The current analysis does not provide evidence on why the models perform in the way they do but suggests that that the spurious increase in high 10–20 year variability from CMIP3 to CMIP5 models may be behind the unsatisfying progress in depicting the spatiotemporal features of the AMO. This problem, coupled with the inability of the models to perturb the regional low-level circulation, the driver of moisture fluxes, seem to be at the center of the poor representation of the hydroclimate impact of the AMO.

References

Booth B, Dunstone NJ, Halloran PR, Andrews T, Bellouin N (2012) Aerosols implicated as a prime driver of twentieth century North Atlantic climate variability. Nature. doi:10.1038/nature10946

Collins WD et al (2006) The community climate system model version 3 (CCSM3). J Clim 19:2122–2143. doi:10.1175/JCLI3761.1

Collins WJ et al (2008) Evaluation of the HadGEM2 model. Met office Hadley centre technical note no. HCTN 74, available from Met Office, FitzRoy Road, Exeter EX1 3 PB http://www.metoffice.gov.uk/publications/HCTN/index.html

Delworth TL et al (2006) GFDL's CM2 global coupled climate models—part 1: formulation and simulation characteristics. J Clim 19:643–674

Donner LJ et al (2011) The dynamical core, physical parameterizations, and basic simulation characteristics of the atmospheric component of the GFDL global coupled model CM3. J Clim 24:3484–3519. doi:10.1175/2011JCLI3955.1

Enfield DB, Mestas-Nunez AM, Trimble PJ (2001) The Atlantic Multidecadal Oscillation and its relation to rainfall and river flows in the continental US. Geophys Res Lett 28:2077–2080

Evan AT, Vimont DJ, Heidinger AK, Kossin JP, Bennartz R (2009) The role of aerosols in the evolution of tropical North Atlantic Ocean temperature anomalies. Science 324:778–781. doi:10.1126/science.1167404

Gent PR et al (2011) The community climate system model version 4. J Clim 24:4973–4991. doi:10.1175/2011JCLI4083.1

Gordon C, Cooper C, Senior CA, Banks H, Gregory JM, Johns TC, Mitchell JFB, Wood RA (2000) The simulation of SST, sea ice extents and ocean heat transports in a version of the Hadley centre coupled model without flux adjustments. Clim Dyn 16:147–168

Griffies SM et al (2011) The GFDL CM3 coupled climate model: characteristics of the ocean and sea ice simulations. J Clim 24:3520–3544. doi:10.1175/2011JCLI3964.1

Guan B, Nigam S (2009) Analysis of Atlantic SST variability factoring inter-basin links and the secular trend: clarified structure of the Atlantic Multidecadal Oscillation. J Clim 22:4228–4240

Hughes SL et al (2009) Comparison on in situ time-series of temperature with gridded sea surface temperature datasets in the North Atlantic. J Mar Sci 66:1467–1479

Hurrell J et al (2010) Decadal climate prediction: opportunities and challenges. In: Hall J, Harrison DE, Stammer D (eds) Proceedings of Ocean Obs'09: sustained ocean observations and information for society (vol. 2), Venice, Italy, 21–25 September 2009, ESA Publication WPP-306

Kavvada A, Ruiz-Barradas A, Nigam S (2013) AMO's structure and climate footprint in observations and IPCC AR5 climate simulations. Clim Dyn. doi:10.1007/s00382-013-1712-1

Kushnir Y, Seager R, Ting M, Naik N, Nakamura J (2010) Mechanisms of tropical Atlantic SST influence on North American precipitation variability. J Clim 23:5610–5628. doi:10.1175/2010JCLI3172.1

Latif M et al (2004) Reconstructing, monitoring, and predicting decadal-scale changes in the North Atlantic thermohaline circulation with sea surface temperature. J Clim 17:1605–1614

Mantua NJ, Hare SR, Zhang Y, Wallace JM, Francis RC (1997) A Pacific interdecadal climate oscillation with impacts on salmon production. Bull Amer Meteor Soc 78:1069–1079

Marsland SJ, Haak H, Jungclaus JH, Latif M, Roeske F (2003) The Max-Planck-Institute global ocean/sea ice model with orthogonal curvilinear coordinates. Ocean Modelling 5:91–127. HAMOCC: technical documentation http://www.mpimet.mpg.de/fileadmin/models/MPIOM/HAMOCC5.1_TECHNICAL_REPORT.pdf

McCabe GJ, Betancourt JL, Gray ST, Palecki MA, Hidalgo HG (2008) Associations of multi-decadal sea-surface temperature variability with US drought. Quat Int 188:31–40. doi:10.1016/j.quaint.2007.07.001

Medhaug I, Furevik T (2011) North Atlantic twentieth century multidecadal variability in coupled climate models: sea surface temperature and ocean overturning circulation. Ocean Sci Discuss 8:353–396

Meehl GA et al (2009) Decadal prediction. Can it be skilful? Bull Amer Meteor Soc 90:1467–1485

Mitchell TD, Jones PD (2005) An improved method of constructing a database of monthly climate observations and associated high resolution grids. Int J Climatol 25:693–712. doi:10.1002/joc.1181

Nigam S, Guan B, Ruiz-Barradas A (2011) Key role of the Atlantic Multidecadal Oscillation in twentieth century drought and wet periods over the great plains. Geophys Res Lett 38:L16713. doi:10.1029/2011GL048650

Pope VD, Gallani ML, Rowntree PR, Stratton RA (2000) The impact of new physical parametrizations in the Hadley Centre climate model–HadAM3. Clim Dyn 16:123–146

Raddatz TJ, Reick CH, Knorr W, Kattge J, Roeckner E, Schnur R, Schnitzler K-G, Wetzel P, Jungclaus J (2007) Will the tropical land biosphere dominate the climate-carbon cycle feedback during the twenty first century? Clim Dyn 29:565–574. doi:10.1007/s00382-007-0247-8

Rayner NA, DE Parker, Horton EB, Folland CK, Alexander LV, Rowell DP, Kent EC, Kaplan A (2003) Global analyses of sea surface temperature, sea ice, and night marine air temperature since the late nineteenth century. J Geophys Res 108(D14):4407. doi:10.1029/2002JD002670

Roeckner E et al (2003) The atmospheric general circulation model ECHAM5. Part I: model description. Max Planck Institute for Meteorology Rep 349, p 127. Available from MPI for Meteorology, Bundesstr. 53, 20146 Hamburg, Germany

Ruiz-Barradas A, Nigam S (2005) Warm season rainfall variability over the US great plains in observations, NCEP and ERA-40 reanalyses, and NCAR and NASA atmospheric model simulations. J Clim 18:1808–1830. doi:10.1175/JCLI3343.1

Shanahan TM, Overpeck JT, Anchukaitis KJ, Beck JW, Cole JE, Dettman DL, Peck JA, Scholz CA, King JW (2009) Atlantic forcing of persistent drought in West Africa. Science 324(5925):377–380. doi:10.1126/science.1166352

Sheffield J et al (2013) North America climate in CMIP5 experiments. Part II: evaluation of historical simulations of intra-seasonal to decadal variability. Submitted to the J Clim

Taylor KE, Stouffer RJ, Meehl GA (2011) An overview of CMIP5 and the experiment design. Bull Amer Meteor Soc 93:485–498. doi:10.1175/BAMS-D-11-00094.1

Ting M, Kushnir Y, Seager R, Li C (2011) Robust features of Atlantic Multidecadal variability and its climate impacts. Geophys Res Lett 38. doi:10.1029/2011GL048712

Wang C, Enfield DB, Lee S-K, Landsea CW (2006) Influences of the Atlantic warm pool on western hemisphere summer rainfall and Atlantic hurricanes. J Clim 19:3011–3028. doi:10.1175/JCLI3770.1

Zhang R, Delworth TL (2006) Impact of Atlantic Multidecadal Oscillations on India/Sahel rainfall and Atlantic hurricanes. Geophys Res Lett 33:L17712. doi:10.1029/2006GL026267

Zhang R et al (2013) Have aerosols caused the observed Atlantic Multidecadal variability? J Atmos Sci 70:1135–1144